Structural and Optical Studies of Fluoride ion binding using *N*-heteroaromatic based ligands.

Priyanka R. Angarkhe[a], Satyajit Sahoo[a], Simran Singhdeo[b], Kripa Shankar SR[c], Manav Upadhyay[c], Kuldeep Mahiya[d], Jagnyaseni Tripathy[b], Rakesh K. Behera[c], Swagat K. Mohapatra[a,*]

[a] *Department of Industrial and Engineering Chemistry, Institute of Chemical Technology - Indian Oil Odisha Campus, Bhubaneswar, Odisha 751013, India.*

[b] *Department of Physics, School of Applied Sciences, KIIT University, Bhubaneswar, Odisha 751024, India.*

[c] *Composite Materials and Mechanics Laboratory, Mechanical and Aerospace Engineering Department, Tandon School of Engineering, New York University, Brooklyn, NY 11201, USA*

[d] *Department of Chemistry, FGM Government College, Adampur, Hisar, Haryana 125052, India.*

Supporting Information

1. Results and Discussion:

Compounds **1**–**3** were readily synthesized according to a modified literature procedure involving a condensation reaction of 1,2-diamino benzene or 2-aminothiophenol with an appropriate aldehyde in the presence of $Na_2S_2O_5$.[1,2] The purity of these compounds was checked using NMR spectroscopy before further analysis.

1.1. Crystal structure of free ligands. Crystals of the free ligands **1**–**3**, suitable for single crystals X-ray diffraction (SCXRD), were grown by slow evaporation of their methanol solution at room temperature. ORTEP plots with crystallographic numbering schemes of their molecular structures and their partial crystal packing diagram with N–H···N and O–H···N (only O–H···N in the case of 2 and 3) hydrogen bonding is shown in Fig. S1. A comparative view of the selected bond lengths and angles of free ligands **1**–**3**, along with those from fluoride complexes **1**-TBAF–**3**-TBAF, is presented in Table S1. It is important to note that the single crystal structure of **2** is known in the literature,[3] but its details are not included in CCDC. Furthermore, additional structural information is not given in the reported literature. A similar pattern of bond distances and bond angles has been observed in all previously reported benzimidazole and benzothiazole derivatives.[1,2,4] Notably, the benzoimidazole and benzothiazole moieties in **1**–**3** are planar, with an average fold angle Φ of 0.4°. Compound **1** exhibits a larger dihedral angle than **2**, and **2** has a larger angle than **3**, characterized by their interplanar angles χ (Table S1). Interestingly, the packing of the structure **1** appears to have a rectangular shape with weak intermolecular H-bonding between N2–H···N1 [*d*(N2–H) = 0.860, *d*(H···N1) = 1.984, *d*(N2···N1) = 2.803 Å, and ∠N2−H···N1 = 158.7 °)] and O1–H…N3 [*d*(O1–H) = 0.820, *d*(H···N3) = 2.306, *d*(O1···N3) = 2.946 Å, and ∠O1−H···N3 = 138.3°] (Fig. S1b), whereas the molecular structure of **2** and **3** shows a chain like packing, with hydrogen bonding O1–H···N3 [*d*(O1–H) = 0.820, *d*(H··· N3) = 2.262, *d*(O1···N3) = 2.888 Å, and ∠O1−H···N3 =

133.5°] for **2** (Fig. S1d), and N2–H···O2 [*d*(N2–H) = 0.860, *d*(H··· O2) = 2.182, *d*(N2···O2) = 2.972 Å, and ∠N2−H···O2 = 152.7°] for **3** (Fig. S1f).

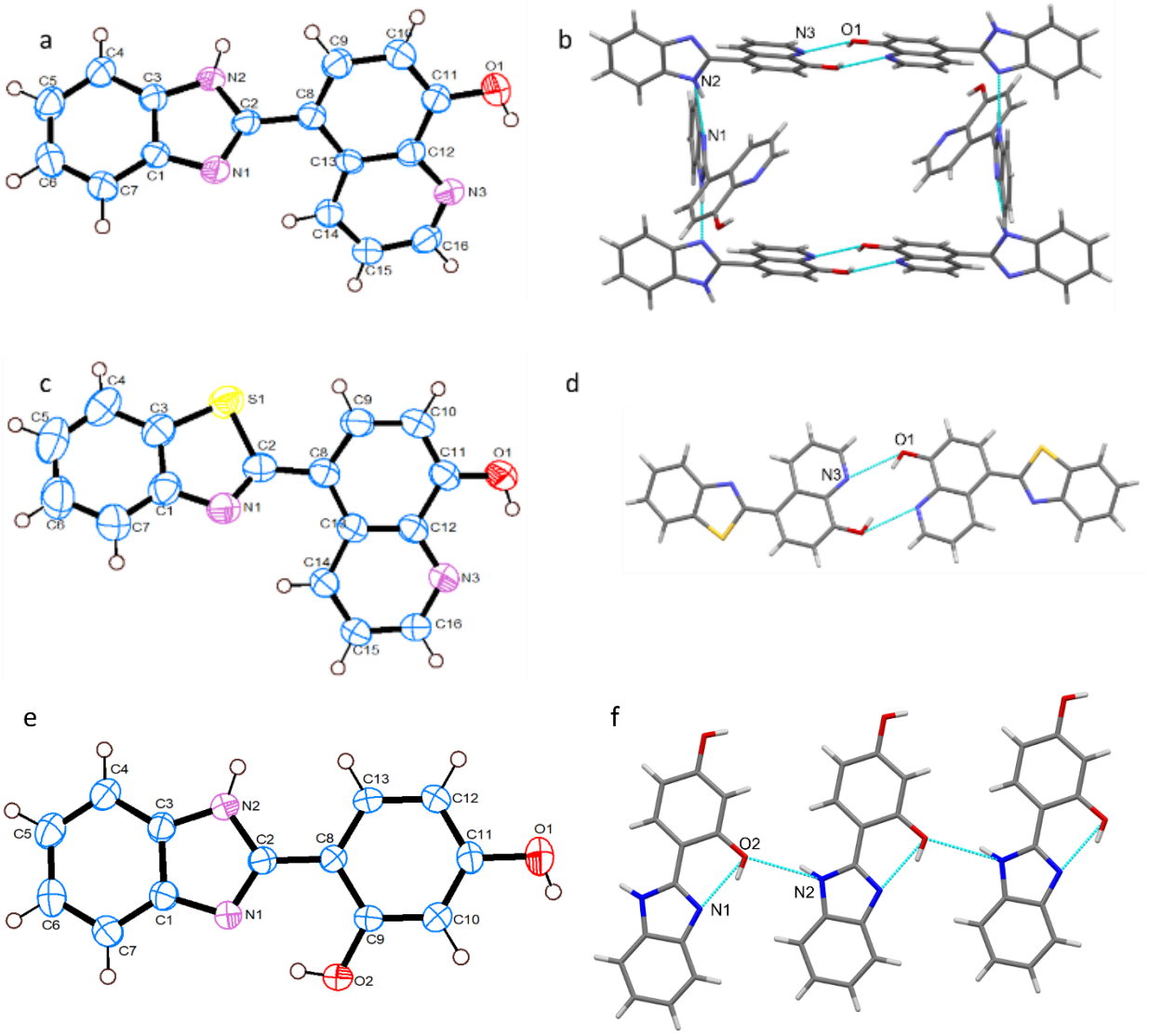

Fig. S1 (a), (c), and (e) are the ORTEP plots of free ligands **1**–**3**, respectively, with anisotropic displacement ellipsoid drawn at 50 % probability; (b), (d), and (f) are the partial views of the crystal packing diagrams showing N–H···N and O–H···N hydrogen bonding interactions (light green color dotted lines) of free ligands **1**–**3**, respectively. Water molecule is removed in the case of **3** for clarity. C–Grey, O–red, S–yellow, N–blue, H–white.

Table S1 Selected bond lengths (Å) and bond angles (°) of free ligands **1**–**3**, and the fluoride complexes **1**-TBAF–**3**-TBAF for comparison.

	N1–C2	N2–C2	S1–C2	O1–C11	Φ[a]	χ[b]
1	1.293(4)	1.334(4)		1.335(4)	0.4	44.5
2	1.294(4)	–	– 1.757(2)	1.345(3)	0.7	24.9
3	1.326(4)	1.364(4)	–	1.386(4)	0.1	0.8
1-TBAF	1.334(3)	1.368(3)	–	1.338(2)	0.6	27.5
2-TBAF	1.306(4)	–	1.767(3)	1.276(4)	2.1	26.4
3-TBAF[c]	1.332(5)	1.373(5)	–	1.350(5)	0.5	2.9
	1.337(5)[d]	1.359(5)[e]	–	1.353(5)[f]	1.0	4.8

[a]*Φ = fold angle between the planes (C1, C3, N1, and N2/S1) and plane (N1, C2, and N2/S1);* [b]*χ = interplanar/dihedral angle between the planes (C1, C3, N1, and N2/S1) and plane (C8, C9, C10, C11, C12, and C13);* [c]*there are two crystallographically independent molecules within the asymmetric unit;* [d]N3–C31; [e]N5–C31; [f]O3–C40.

1.2. Structural description of a distorted cubical fluoride-water cluster $[F_2(H_2O)_8]^{2-}$, seen in the molecular structure of 3-TBAF.

The molecular structure of $[F_2(H_2O)_8]^{2-}$comprises two crystallographically inequivalent molecules $[F_2(H_2O)_8]^{2-}$ (**I**) (Fig. 4d), and $[F_2(H_2O)_8]^{2-}$(**II**) (Fig. 4e), each displaying a rather different geometry. Notably, there are several well-established reports available on fluoride-water cluster complexes.[5–10] Both the cluster units are entirely encapsulated within the cavity of a total four-receptor molecules (two each from the two molecules, geometrically inequivalent, present in the asymmetric unit), forming a total of six H-bonded contacts, two each from N−H···F, O−H···F and O···H−O. As shown in Fig. 4d and e, the cluster complex has a geometry more towards a distorted cubical structure, with a range of ∠O−O−O bond angle from 84.7 to 103.2° (Table S2). Each cluster is made up of two symmetrical units of $F^-.4H_2O$, where two quadrilateral faces in **I** (Fig. 4d), and **II** (Fig. 4e) are stacked on each other parallelly, with an average contact distance between their

centroids is 3.419 Å ($Ct_{O9–O10–O11–O12}$–$Ct_{O9–O10–O11–O12}$ = 3.334 (**I**), and $Ct_{O5–O6–O7–O8}$–$Ct_{O5–O6–O7–O8}$ = 3.5053 Å (**II**)). The pressure is applied on the nodes O11 and O12 (**I**), and O7 and O8 (**II**) vertically, and the water cubical sphere is pulled more towards the F^- ion. Among the eight central H_2O molecules from the cubical sphere of **I**, six molecules form three H-bonds, two acceptors, and one donor, while two molecules form four H-bonds, two-acceptor, and two-donor. While in **II**, six H_2O molecules are having three H-bonds same as cluster I, and two molecules are having only two H-bond, one acceptor and one donor.

Table S2 Geometrical parameters of the fluoride-water cluster complexes $[F_2(H_2O)_8]^{2-}$ (**I**) and $[F_2(H_2O)_8]^{2-}$ (**II**) (Fig. 4d and e).

$[F_2(H_2O)_8]^{2-}$ (**I**)				$[F_2(H_2O)_8]^{2-}$ (**II**)			
(a) H-bond distances (Å) and angles (°) to the central F^- ion							
D···F	*d*(D···F)	D···F···D	∠D···F···D	D···F	*d*(D···F)	D···F···D	∠D···F···D
O3···F1	table 2	O11···F1···O12	84.1	O1···F2	table 2	O7···F2···O8	86.0
N2···F1	table 2	O11···F1···O3	104.1	N5···F2	table 2	O8···F2···O1	113.8
O12···F1	2.703(4)	O12···F1···N2	111.8	O7···F2	2.762(4)	O7···F2···N5	106.2
O11···F1	2.805(4)	O3···F1···N2	119.8	O8···F2	2.686(4)	O1···F2···N5	123.6
(b) H-bond distances (Å) and angles (°) to the central H_2O deformed cube							
O···O	*d*(O···O)	O···O···O	∠O···O···O	O···O	*d*(O···O)	O···O···O	∠O···O···O
O11···O10	2.839(5)	O11···O10···O12	92.7	O7···O5	2.862(5)	O7···O5···O8	91.6
O10···O12	2.885(6)	O10···O12···O9	86.1	O5···O8	2.815(5)	O5···O8···O6	87.1
O12···O9	2.786(6)	O12···O9···O11	93.4	O8···O6	2.824(6)	O8···O6···O7	93.2
O9···O11	2.906(6)	O9···O11···O10	84.7	O6···O7	2.778(5)	O6···O7···O5	86.9
O9···O10	3.036(8)	O11···O10···O9	91.9				
		O12···O10···O9	103.2				
		O10···O9···O12	101.6				
		O10···O9···O11	89.9				

1.3. Additional NMR details.

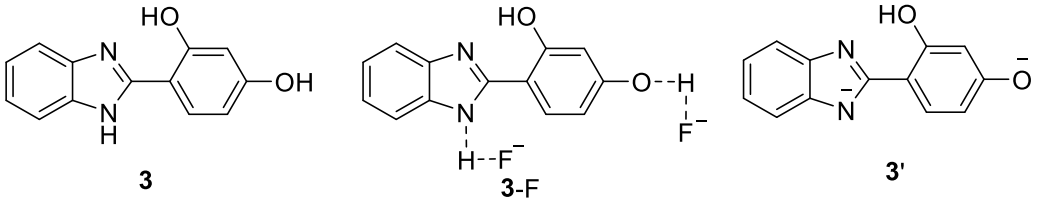

Figure S2: Showing binding modes between the receptor molecule **3** and F^- ion.

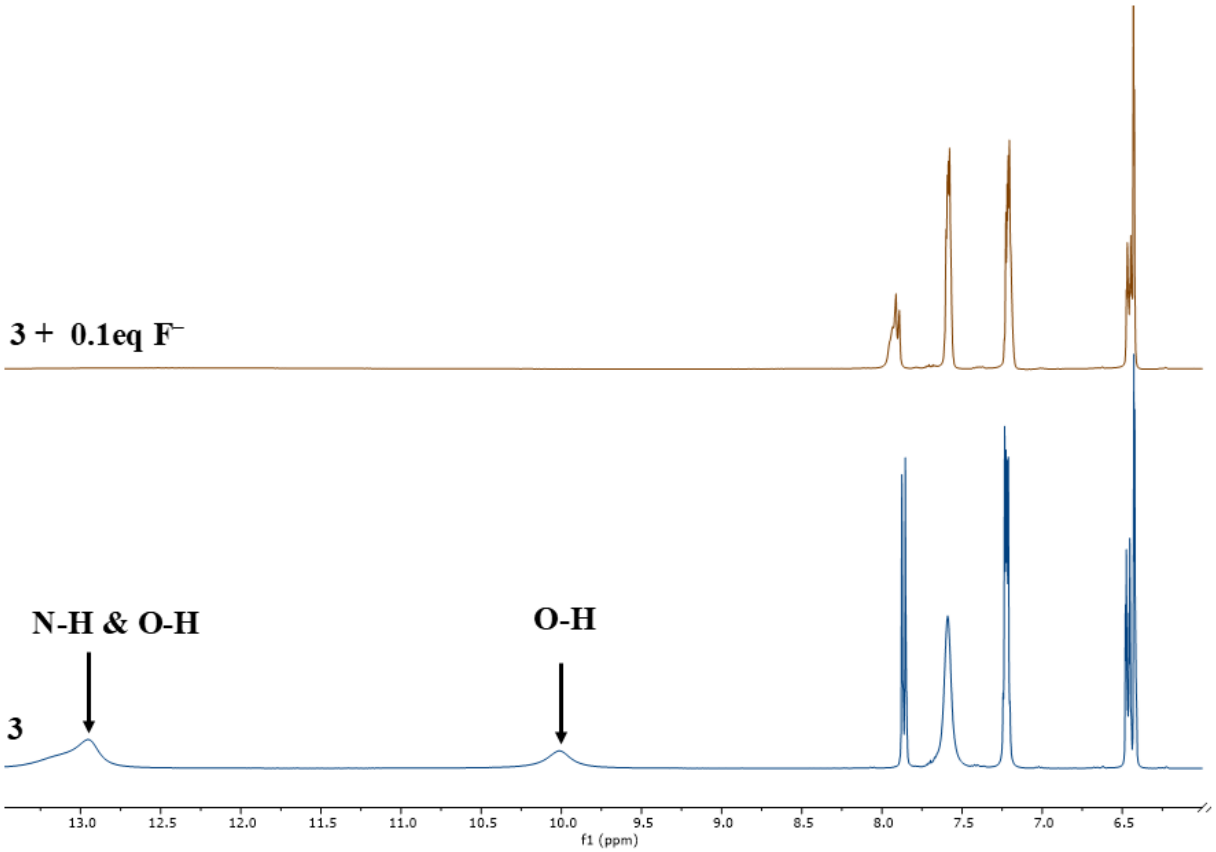

Figure S3: A partial view of the ^{1}H NMR in DMSO-d_6 (bottom), recorded for the receptor molecule **3** and after addition of 1 equivalent of TBAF (top).

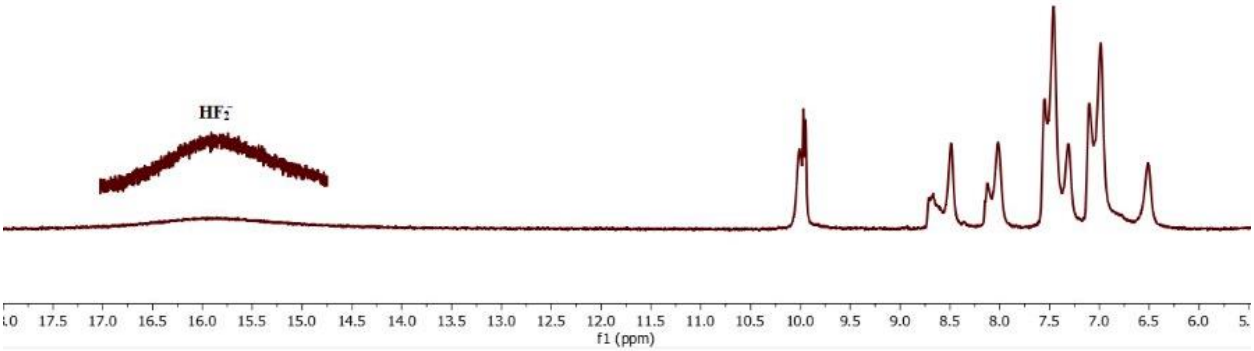

Figure S4: A partial view of the ^{1}H NMR in DMSO-d_6 (bottom), recorded for the mixture of receptor molecule **1** and TBAF (ratio 1:3), highlighting the HF_2^- peak.

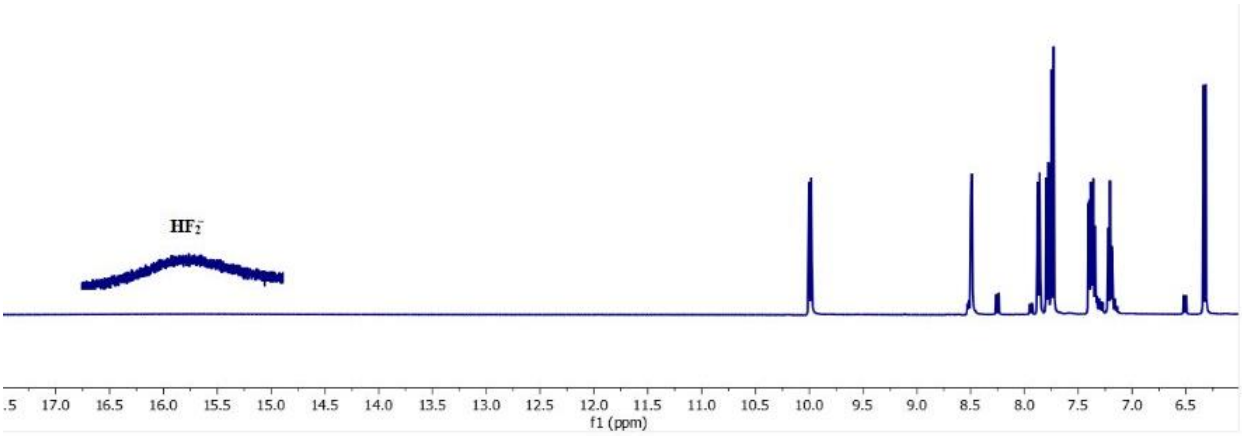

Figure S5: A partial view of the ^{1}H NMR in DMSO-d_6 (bottom), recorded for the mixture of receptor molecule **2** and TBAF (ratio 1:4), highlighting the HF_2^- peak.

1.4. UV-Vis details.

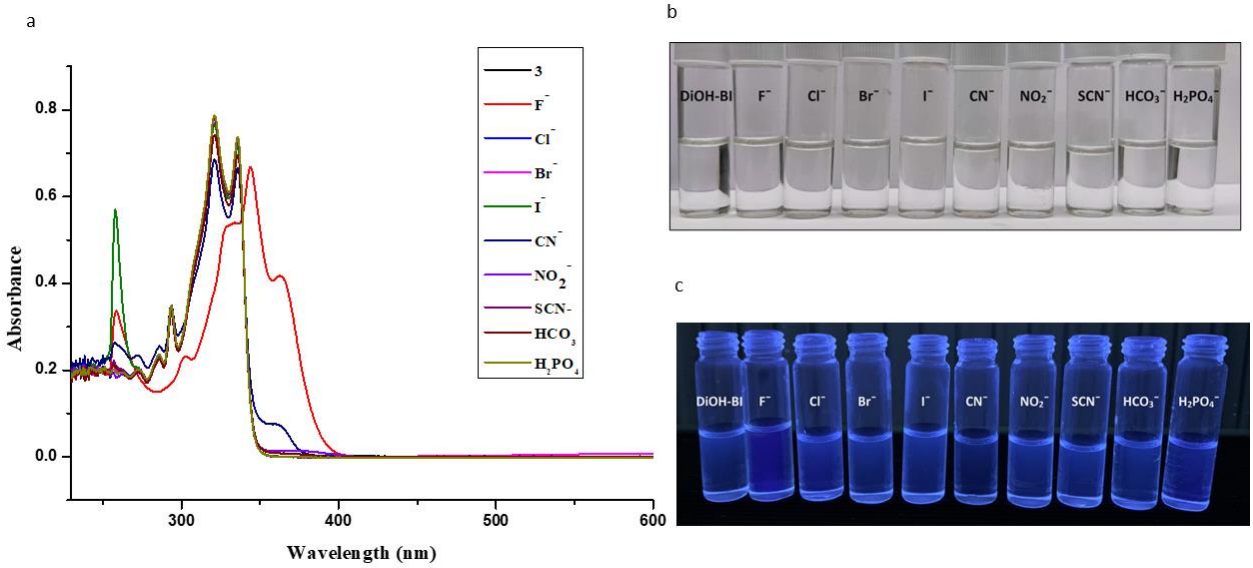

Figure S6: (a) Changes in the UV-Vis spectral features of **3** (DiOH-BI) in DMSO upon the addition of TBA^+ salts of different anions with a ratio of 1:100. (b) and (c) Observation of color changes in visible and UV light that occurred in **3** in DMSO after adding the TBA^+ salts of different anions. [**3**] = 30 μM.

1.5. Additional HS analysis details.

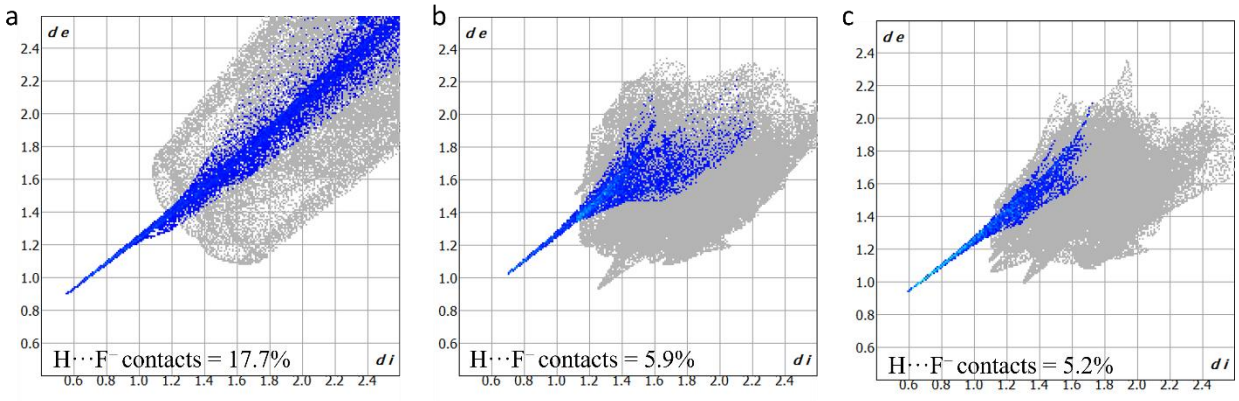

Figure S7: (a), (b), and (c) show the 2D fingerprint plots of the perentage contribution of H···F⁻ contacts to the HS of **1**-TBAF-**3**-TBAF.

1.6. Additional Computational details.

Crystal Structures. The crystal structure details (lattice parameter, space group) of all the three systems are shown in Table S3.

Table S3. Crystal structure, K-points used and predicted Band Gap of all the three systems.

System	Unit Cell Parameters (lengths are in Å and angles are in °)	Space Group
1-TBAF	a = 8.2214, b = 17.6870, c = 23.1490 α = 90.000, β = 97.908, γ = 90.000	P 2_1/n
2-TBAF	a = 8.2612, b = 9.5452, c = 9.9777 α = 94.986, β = 93.564, γ = 98.378	P-1
3-TBAF	a = 19.9390, b = 16.4070, c = 20.1470 α = 90.000, β = 97.563, γ = 90.000	P 2_1/c

For each crystal structure, the view is shown along the a, *b*, and *c* axis in a capped stick format where the F atoms are highlighted in each unit cell (Figures S8-S10).

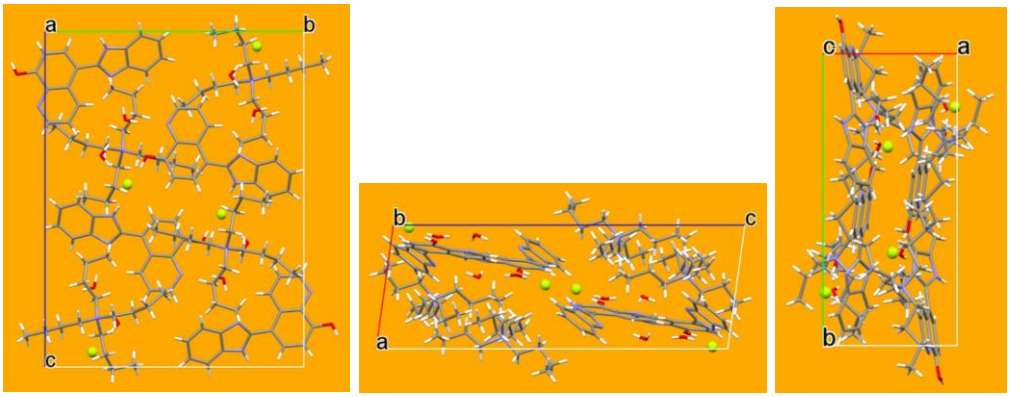

Figure S8. a, b, and c-axis view of **1**-TBAF unit cell with P $2_1/n$ space group symmetry.

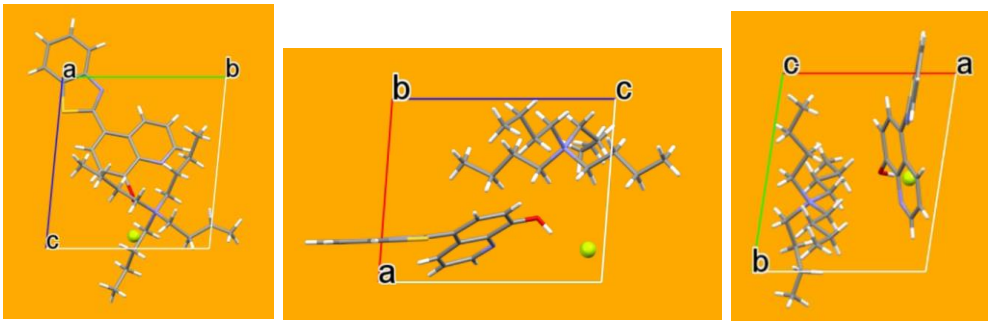

Figure S9. a, b, and c-axis view of **2**-TBAF unit cell with P-1 space group symmetry.

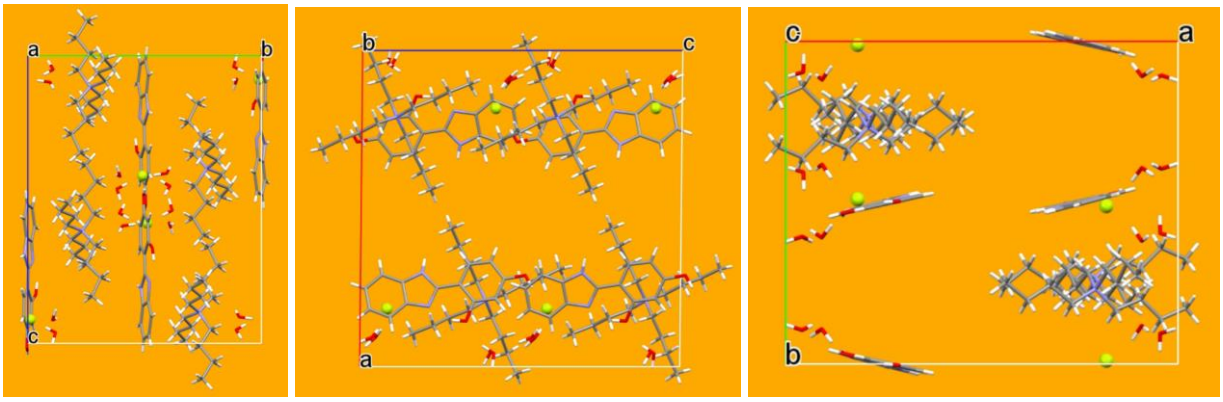

Figure S10. a, b, and c-axis view of **3**-TBAF unit cell with P $2_1/c$ space group symmetry.

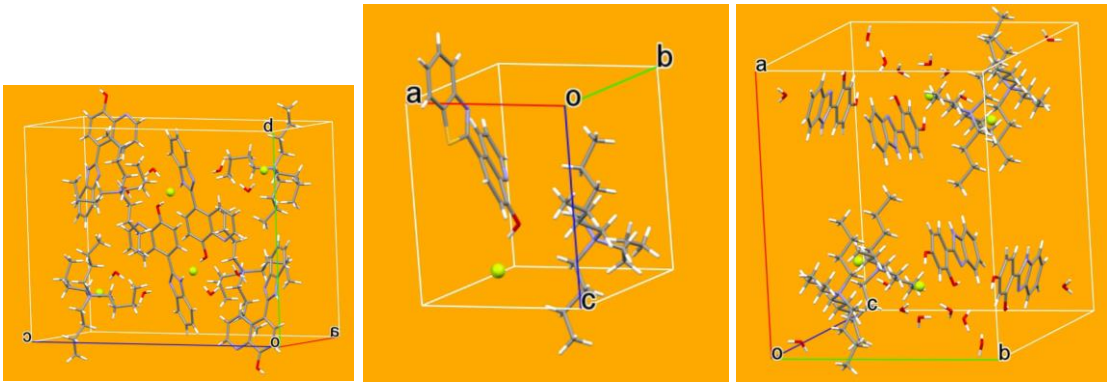

Figure S11. Crystal structure of **1**-TBAF (left), **2**-TBAF (middle), and **3**-TBAF (right) unit cells in capped stick format.

The band structure, total density of states (TDOS) and partial density of stated (PDOS) of all the three systems are shown in Figures S12 – S14.

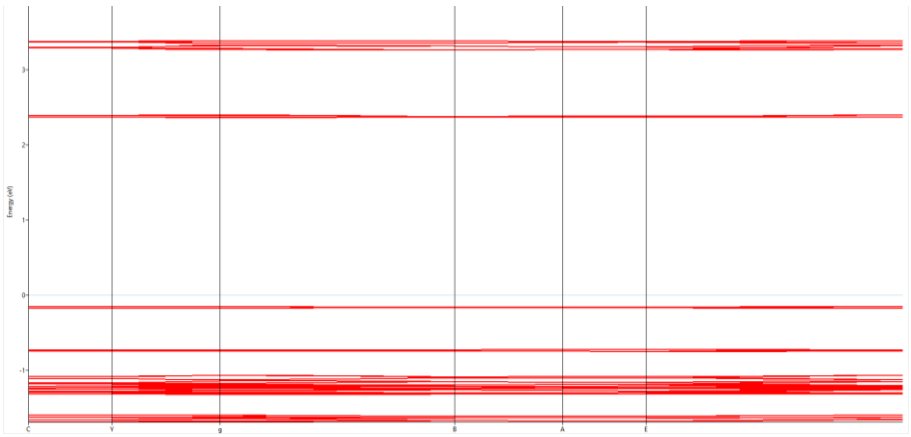

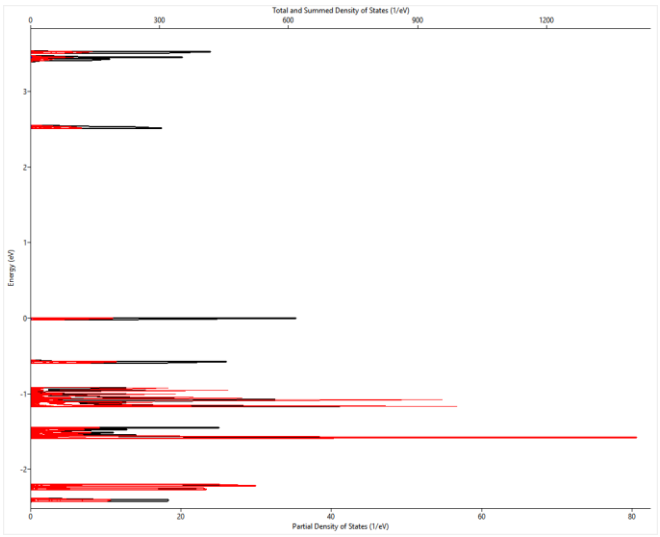

Figure S12. Band Structure and Total/Partial Density of States of **1**-TBAF showing discrete bands present in the crystalline system with a large band gap. For DOS, Fermi Energy is shifted to 0 eV.

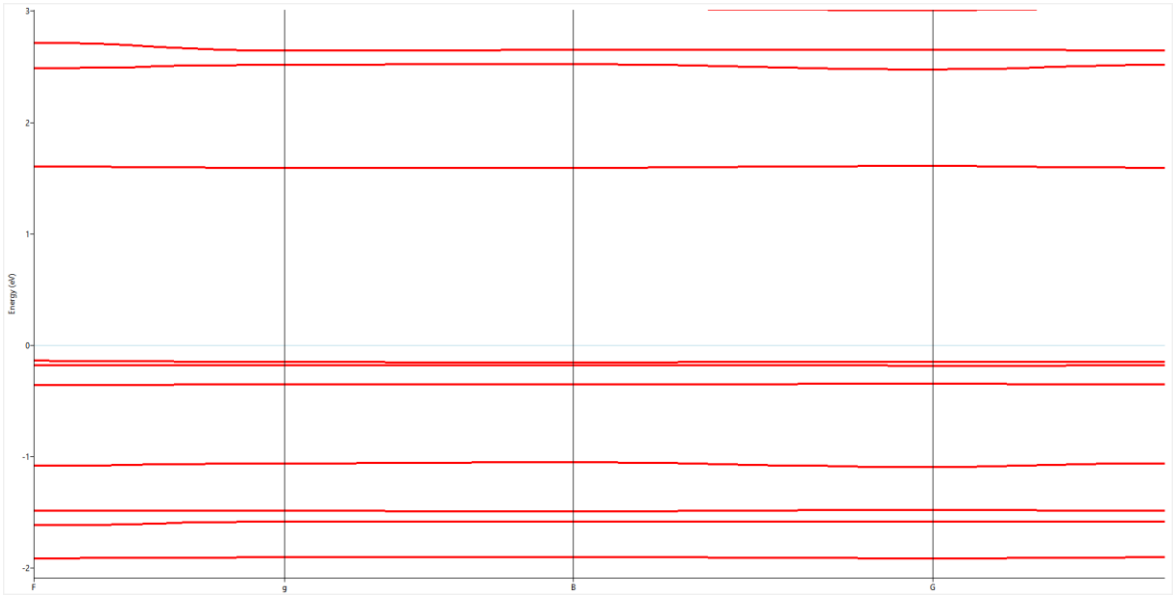

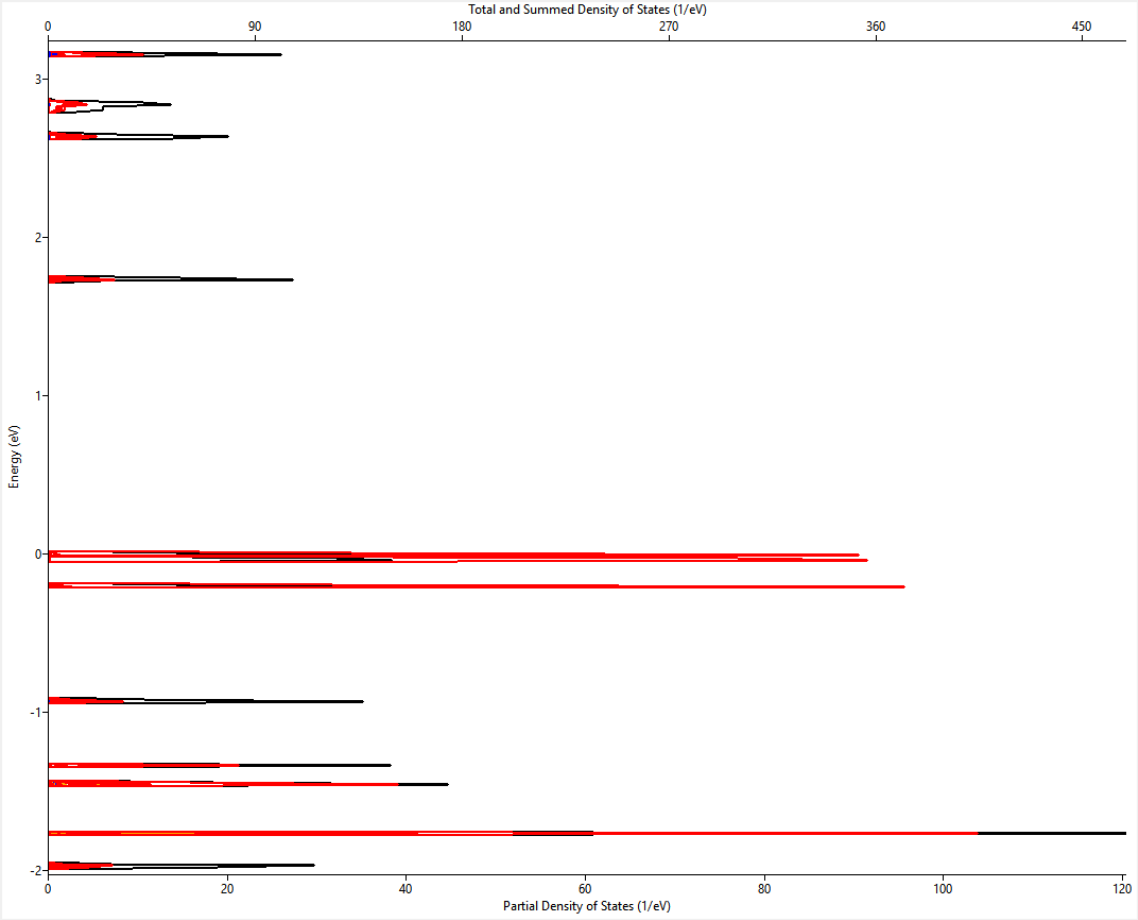

Figure S13. Band Structure and Total/Partial Density of States of **2**-TBAF showing discrete bands present in the crystalline system with a large band gap. For DOS, Fermi Energy is shifted to 0 eV.

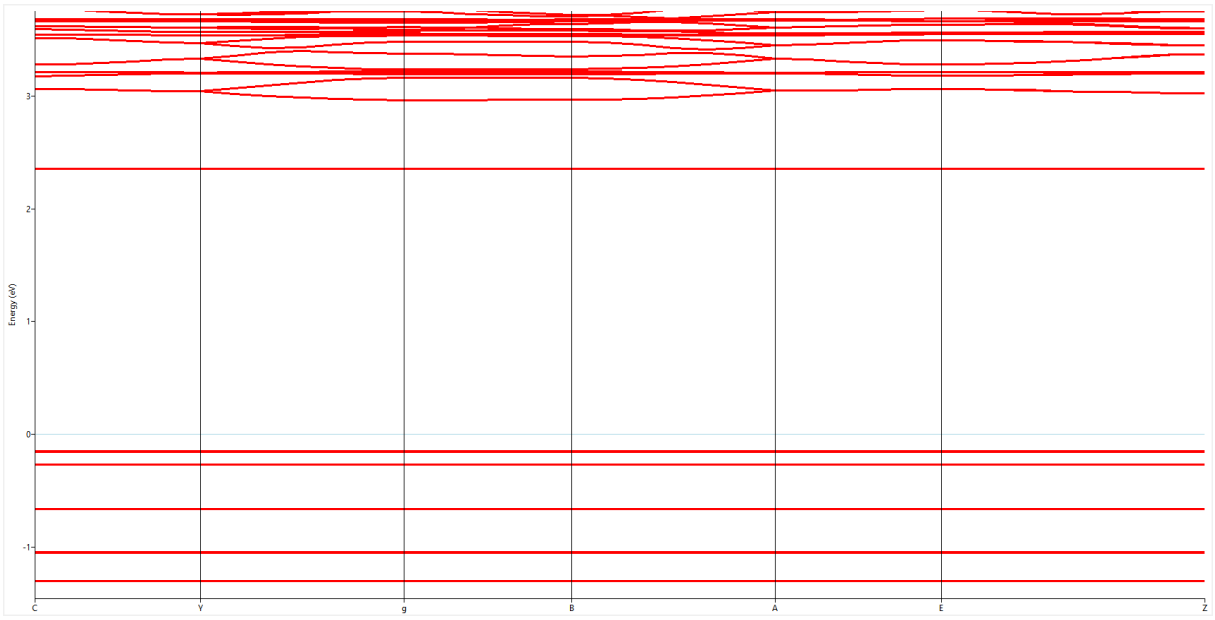
Energy (eV)
3
2
1
0
-1
C
Y
g
B
A
E
Z

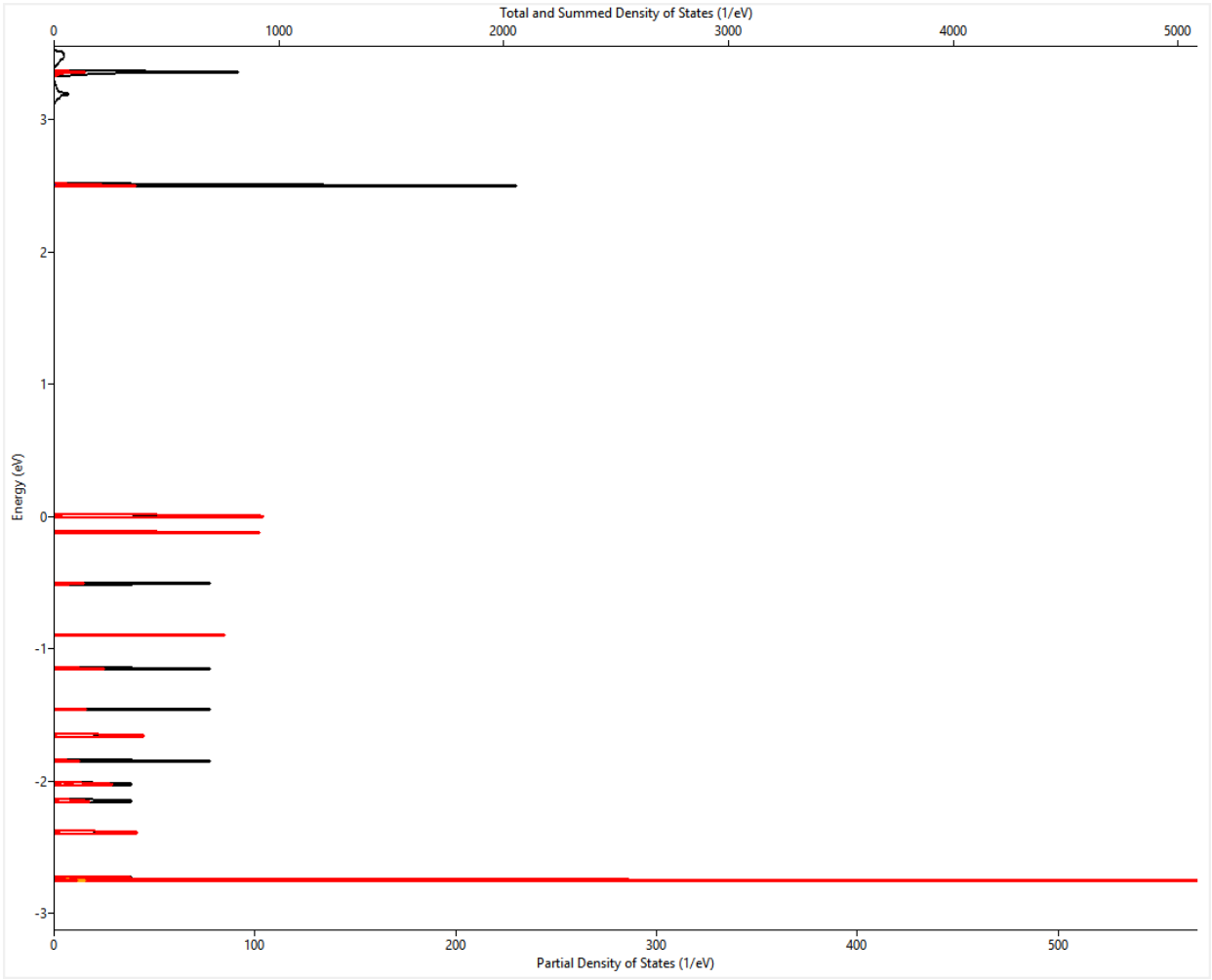
Total and Summed Density of States (1/eV)
0
1000
2000
3000
4000
5000
Energy (eV)
3
2
1
0
-1
-2
-3
0
100
200
300
400
500
Partial Density of States (1/eV)

Figure S14. Band Structure and Total/Partial Density of States of **3**-TBAF showing discrete bands present in the crystalline system with a large band gap. For DOS, Fermi Energy is shifted to 0 eV.

In order to eliminate the selected GGA-PBE functional, we also performed the electronic structure studies of **2**-TBAF with other functionals and approximations such as GGA+BLYP with Grimme's D2 correction to include dispersion, van der Waals density functional with rVV10L, van der Waals density functional with revPBE-vdW functional.

Table S4. Summary of all the different Functionals and exchange-correlation approximations used to estimate the band structure of **2**-TBAF.

Functional	Exchange-Correlation	Additional computational set-up	Predicted Band Gap in eV
Density Functional	GGA-PBE		1.71
Density Functional	GGA-BLYP	DFT+D2	1.87
vdW Density Functionl	PBE+rVV10L		1.76
vdW Density Functionl	revPBE-vdW		1.79

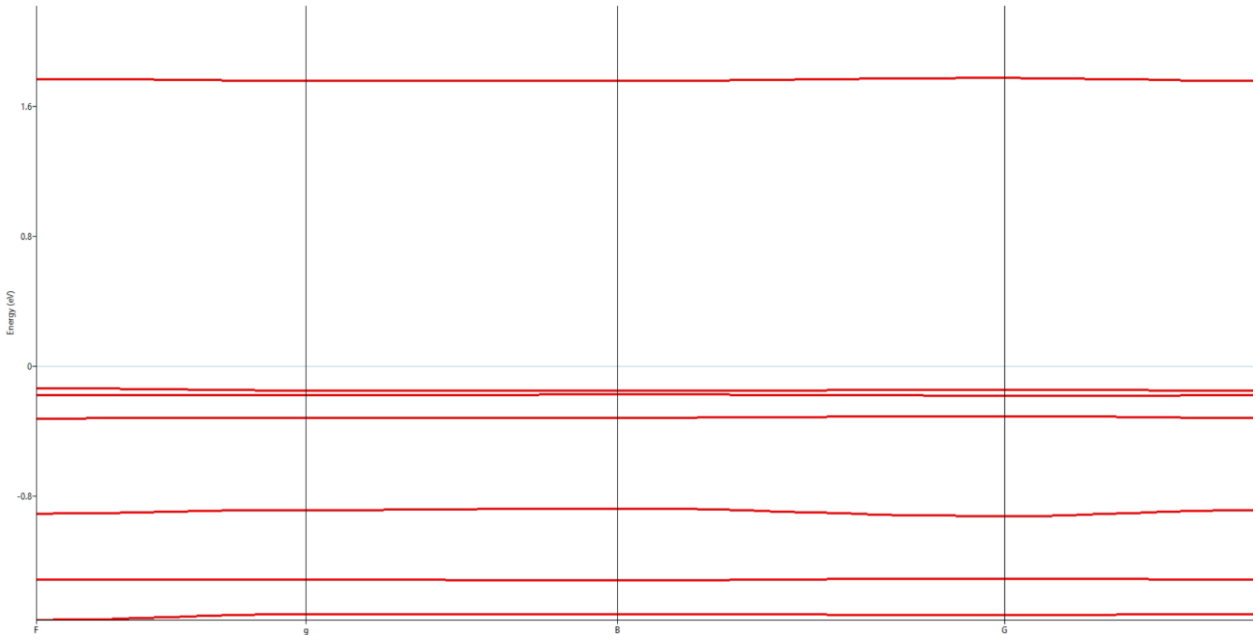

Figure S15. Band Structure predicted by DFT+BLYP with D2 correction.

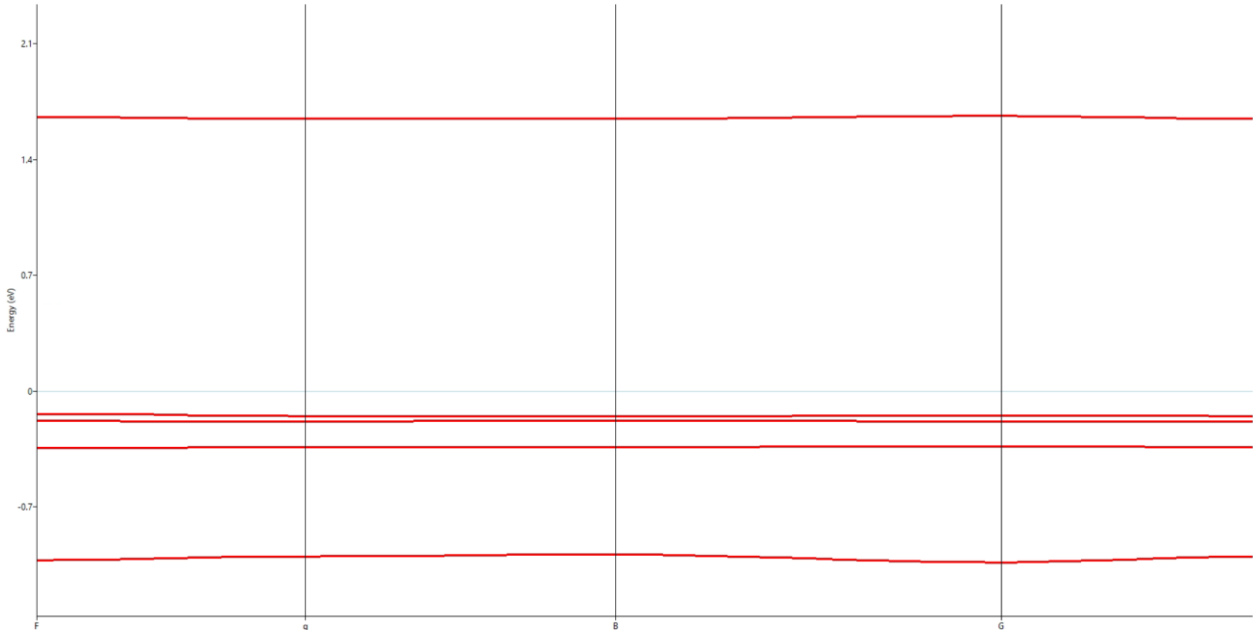

Figure S16 Band Structure predicted by van der Waals density functional PBE + rVV10L for describing the interactions.

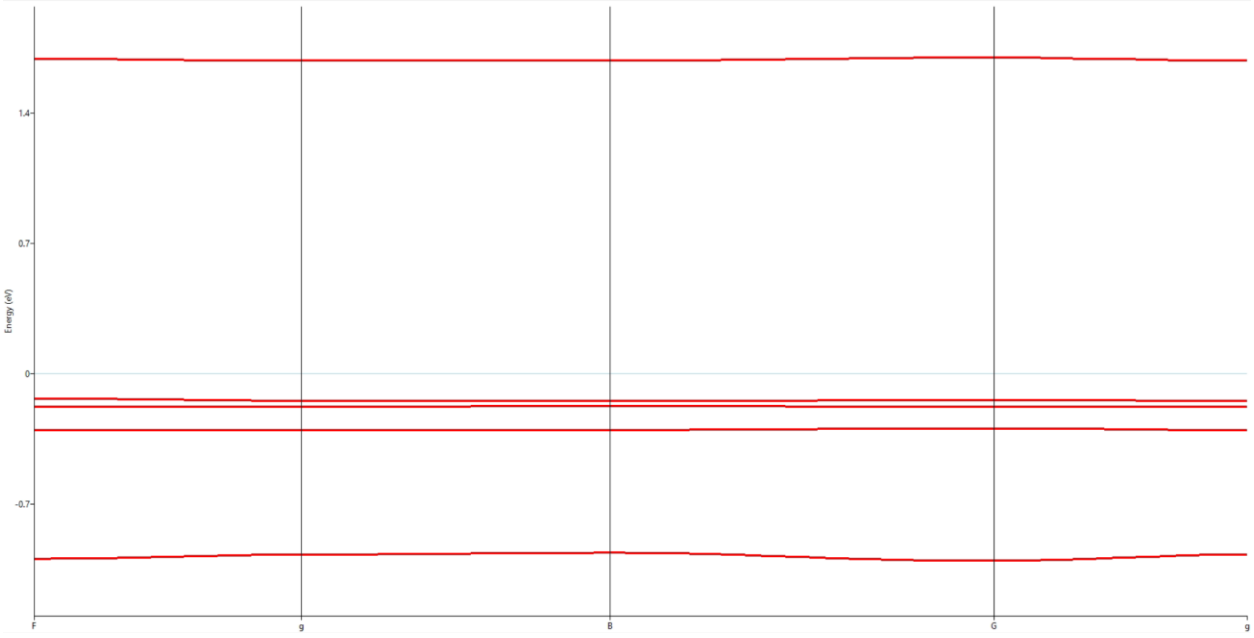

Figure S17 Band Structure predicted by van der Waals density functional revPBE-vdW for describing the interactions.

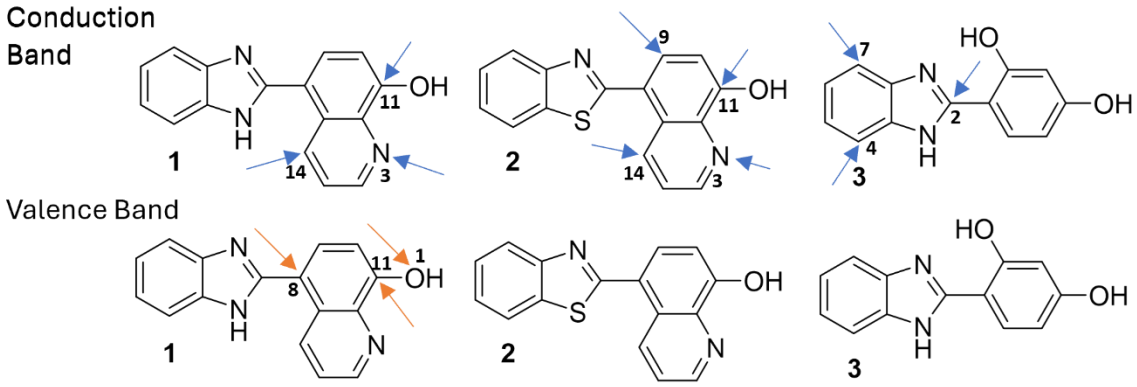

Figure S18. The conduction band and valence band are primary contributors to all the receptors.

The complete cell optimization result of **2**-TBAF is shown in Table S2. This shows the cell volume and cell dimension have increased overall after the optimization. We have used the optimized cell parameters to estimate the optical response of **2**-TBAF.

Table S5. Atomic position, cell volume and cell shape optimization of **2**-TBAF using GGA-PBE pseudopotential.

System	Unit Cell Parameters (lengths are in Å and angles are in °)	Volume in Å^3
2-TBAF	a = 8.2612, b = 9.5452, c = 9.9777 α = 94.986, β = 93.564, γ = 98.378	773.210
2-TBAF GGA-PBE Optimized	a = 8.4536, b = 9.9209, c = 10.0924 α = 96.448, β = 93.588, γ = 98.455	829.136

The optical response of **2**-TBAF including absorbance, transmittance and reflectance is shown in Figure S16. The highest sensitivity to optical response is observed to be in the x-direction.

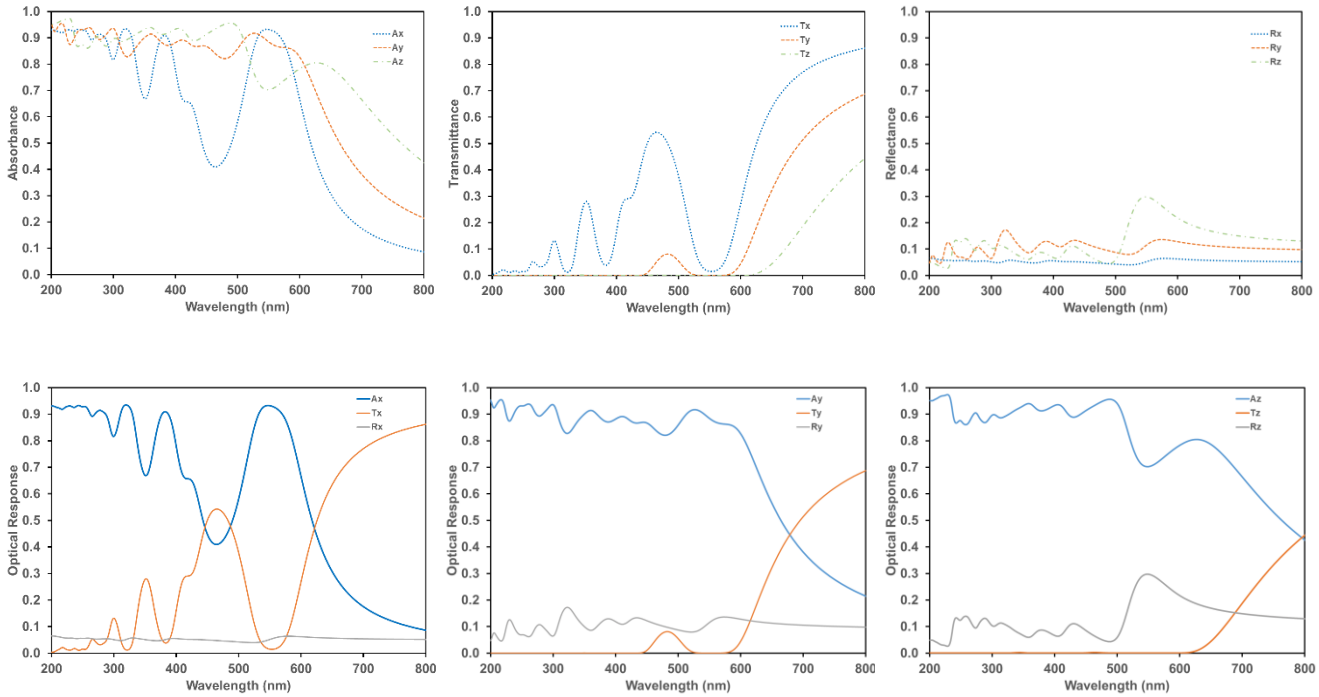

Figure S19. Optical response of optimized **2**-TBAF crystal showing absorption, transmission, and reflection in the visible wavelength range. The directional optical response is show here as well.

A closer look at the crystal stacking shows that the molecules are stacked along the x-axis (Figure S20), leading to a stronger optical response. The receptor molecules are arranged side-by-side along the y- and z- direction (Figure S20), leading to a lesser sensitivity to optical stimuli.

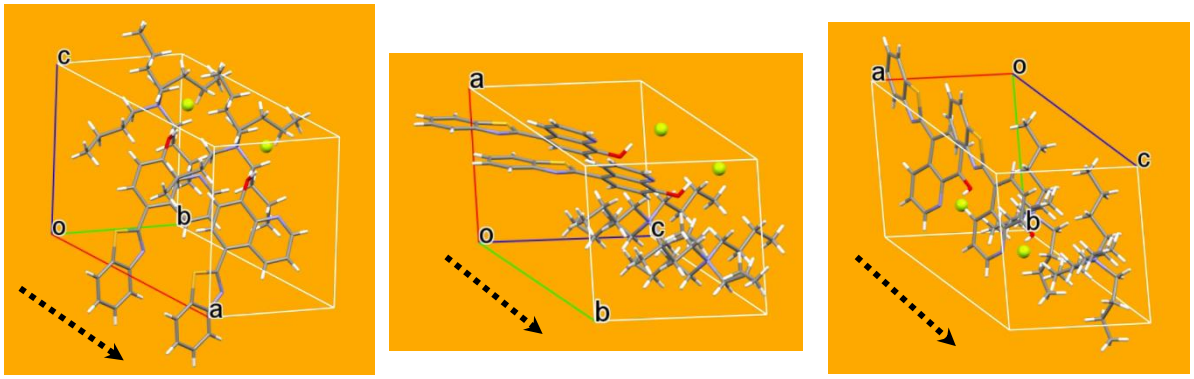

Figure S20. Crystal packing along *a*-, *b*-, and *c*-direction corresponding to *x*-, *y*-, *z*-axis respectively for **2**-TBAF crystal. The arrows in each periodic arrangement shows the primary direction of evaluation. A 2 x 1 x 1 supercell (2 units along *a*-, 1 unit along *b*- and 1 unit along *c*-axis) is plotted for analyzing the packing in the *a*-direction, a 1 x 2 x 1 supercell is plotted for analyzing the packing in the *b*-direction, and a 1 x 1 x 2 supercell is plotted for analyzing the packing in the *z*-direction.

2. Experimental

2.1. General experimental procedure. All operations were conducted in an aerated atmosphere. Commercially available chemicals, including solvents, were used as is. The synthesis of 5-formyl-8-hydroxyquinoline followed the procedure described in the literature.[11] The compounds 1, 2 and 3 were synthesized using modified literature procedures.[1,2] ^{1}H and $^{13}C\{^{1}H\}$ NMR spectra were recorded on Bruker Advance 400 MHz spectrum. They were referenced to tetramethylsilane using

the residual proton signal of the solvent and the carbon resonances of the deuterated solvent, respectively. UV-Vis absorption spectra were recorded in a JASCO V-770 UV-Vis spectrophotometer.

2.2. Synthesis of 1. 1,2-Diaminobenzene (0.5 g, 4.6 mmol) 5-formyl-8-hydroxyquinoline (0.8 g, 4.7 mmol) and sodium pyrosulfite (1.76 g, 9.2 mmol) were heated under reflux in a mixture of 50 mL of ethanol and water (9:1) for 2 hours. The reaction progress was monitored using TLC. The resulting mixture was concentrated using a rotary evaporator, and then water was added to precipitate the product. The obtained olive green solid was filtered and washed thoroughly with hot hexane to yield the desired product (0.85 g, 70 % yield). NMR data were consistent with the previous report.[12]

2.3. Synthesis of 2. It was prepared by reacting between 2-aminothiophenol (0.5 g, 4.0 mmol), 5-formyl-8-hydroxyquinoline (0.7 g, 4.0 mmol), and sodium pyrosulfite (1.5 g, 8 mmol), following the procedure given for **1**. Color: light brown solid, yield: 0.65 g (58 %): NMR data were consistent with the previous report. [3]

2.4. Synthesis of 3. It was prepared by reacting between 1,2-Diaminobenzene (0.5 g, 4.6 mmol), 2,4-dihydroxybenzaldehyde (0.65 g, 4.7 mmol), and sodium pyrosulfite (1.76 g, 9.2 mmol), following the procedure given for **1**. Color: yellow color solid, yield: 0.9 g (86 %): 1H and 13C NMR data were consistent with the previous report.[13]

2.5. General procedure for fluoride complex synthesis and crystallization of 1-TBAF–3-TBAF. The fluoride receptors (**1**–**3**,10 mg) and TBAF.3H_2O with a 1:1 molar ratio was dissolved in 5 mL mixture solution of dichloromethane and methanol (1:1). The solution was then left

undisturbed for slow evaporation at room temperature to grow crystals suitable for single crystal X-ray analysis.

2.6. X-ray crystallography. The X-ray diffraction studies were carried out with a Bruker Apex-II CCD area detector diffractometer, using graphite-monochromated Mo K radiation (λ = 0.71073 Å). The intensity data were processed using the Bruker suite of data processing program (SAINT) (SAINT; Bruker AXS, I, analytical X-ray system 2000,5373). Empirical absorption corrections were applied using the SADABS program (SADABS; Siemens Industrial Automation, I. 1996). All the structures were solved by direct method and refined by the full-matrix least-squares of F^2 using the SHELXTL-PLUS software.[14] All the non-hydrogen atoms were refined anisotropically, while hydrogen atoms were refined in an idealized position and then refined riding on the carbon atoms with isotropic displacement parameters U(H) = 1.2U_{eq}. Table S6 represents all the crystal data and structure refinement parameters.

Table S6: Crystal data and structural refinement parameters.

	1	**2**	**3**	**1**-TBAF.2H_2O	**2**-TBAF	**3**-TBAF.4H_2O
CCDC No	2387451	2387452	2394711	2387453	2387454	2387455
Exp Formula	$C_{16}H_{11}N_3O$	$C_{16}H_{10}N_2OS$	$C_{13}H_{11}N_2O_{0.5}$	$C_{32}H_{49.55}FN_4O_3$	$C_{32}H_{46}FN_3OS$	$C_{29}H_{54}FN_3O_6$
Crystal color/shape	Yellow/ Plate	Yellow/ Rod	Colorless/ Plate	Yellow/ Plate	Yellow/ Block	Colorless/ Plate
Crystal size / mm^3	0.20×0.19×0.18	0.22×0.20×0.18	0.21×0.20×0.19	0.2×0.19×0.18	0.19×0.18×0.17	0.2×0.19×0.18
FW	261.28	278.32	235.24	558.76	539.78	559.75
Crystal system	Monoclinic	Triclinic	Triclinic	Monoclinic	Triclinic	Monoclinic
T, K	299(2)	299(2)	298(2)	299.00	299(2)	299.15
Space group	C2/c	P -1	P -1	$P2_1/n$	P-1	$P2_1/c$
a / Å	41.92(4)	8.0639(10)	3.8217(9)	8.2214(14)	8.2612(12)	19.939(7)
b / Å	5.948(5)	8.1559(11)	5.7898(11)	17.687(3)	9.5452(14)	16.407(5)
c / Å	9.899(11)	10.4359(14)	24.196(5)	23.149(3)	9.9777(12)	20.147(6)
α / °	90	99.948(5)	94.416(7)	90	94.986(4)	90
β / °	94.88(4)	108.024(4)	91.100(9)	97.908(5)	93.564(4)	90.563(12)
γ / °	90	96.408(5)	93.667(8)	90	98.378(5)	90
V / $Å^3$	2460(4)	632.80(14)	532.5(2)	3334.1(9)	773.21(19)	6591(4)
Z	8	2	2	4	1	8
ρ_{calc} / g cm^{-3}	1.412	1.461	1.467	1.110	1.159	1.128
μ / mm^{-1}	0.092	0.251	0.104	0.075	0.139	0.082

Abs. corr. T_{max},	0.984,	0.956,	0.980,	0.987,	0.977,	0.985,
T_{min}	0.982	0.946	0.978	0.985	0.974	0.984
F(000)	1088	288.0	246.0	1210	292.0	2448.0
Index ranges	–50≤ h ≤50	–10≤ h ≤10	–4≤ h ≤4	–9 ≤ h ≤ 9	–10 ≤ h ≤ 10	–23 ≤ h ≤ 23
	–7≤ k ≤7	–10≤ k ≤10	–7≤ k ≤7	–21 ≤ k ≤ 21	–12 ≤ k ≤ 12	–19 ≤ k ≤ 19
	–11≤ l ≤12	–13≤ l ≤13	–31≤ l ≤31	–27 ≤ l ≤ 27	–10 ≤ l ≤ 12	–23 ≤ l ≤ 23
2θ range / °	5.852–51.788	5.396–55.058	5.068–55.128	4.936–50.0	4.334–55.182	4.512–50.0
Total refs	2388	20160	53905	44154	18283	61333
Ind. refs (R_{int})	2261 (0.1177)	2915 (0.0891)	2435 (0.0914)	5837 (0.0786)	0.0680, (0.1375)	11601 (0.2001)
Refs with I > 2σ(I)	9972	20160	8067	44154	18283	61333
Data/restraints/ parameters	2261/0/183	2915/0/182	2435/1/166	5837/211/451	6329/41/377	11601/1/735
GOF (F^2)	1.086	1.105	1.084	1.076	1.051	0.864
$R_1(F)$, $wR_2(F^2)$ [I > 2σ(I)]	0.0680, 0.1376	0.0496, 0.1111	0.0695, 0.1450	0.0594, 0.1739	0.0574, 0.1087	0.0776, 0.1732
$R_1(F)$, $wR_2(F^2)$ [all data]	0.0680, 0.1796	0.0496, 0.1437	0.0695, 0.2003	0.0594, 0.1977	0.0574, 0.1245	0.0776, 0.2291
largest peak, hole / e Å^{-3}	0.26, –0.29	0.20, –0.29	0.25, –0.27	0.24, –0.17	0.20, –0.15	0.18, –0.32

2.6. Computational details. Density functional theory (DFT) at the level of plane waves was used for all of the calculations performed on the Pb and Pb–C systems in this work. The DFT calculations were carried out using the Vienna Ab initio Simulation Package (VASP)[15,16] available within the MedeA Platform.[17] The generalized gradient approximation (GGA) functional parametrized by Perdew, Burke, and Ernzerhof (PBE) was used to describe the exchange and correlation energies of the electrons.[18] The projector-augmented wave (PAW) pseudopotentials described the valence electron configurations of $1s^1$, $2s^22p^2$, $2s^22p^3$, $2s^22p^4$, $2s^22p^5$, and $3s^23p^4$ for H, C, N, O, F, and S, respectively. All of the calculations performed for this computational examination used a plane-wave cutoff energy of 500 eV, where electronic relaxation was completed with a self-consistent field (SCF) convergence of 1.0×10^{-6} eV. The unit cell details of all the three structures along with different k-point Monkhorst–Pack meshes used for integrations over the Brillouin zone[19] is presented in Table S7. The actual k-spacing maintained in the unit of 1/Å for all the three systems is also reported in the Table 7 for all of the structures.

Table S7 Crystal structure, K-points used and predicted Band Gap of all the three systems.

System	Unit Cell Parameters (lengths (Å) and angles (°))	k-point Mesh (k-spacing in 1/Å)	Band Gap (in eV)
1-TBAF	a = 8.2214, b = 17.6870, c = 23.1490 α = 90.000, β = 97.908, γ = 90.000	4 x 2 x 4 (0.193 x 0.178 x 0.069)	2.52 (indirect)
2-TBAF	a = 8.2612, b = 9.5452, c = 9.9777 α = 94.986, β = 93.564, γ = 98.378	4 x 3 x 3 (0.193 x 0.223 x 0.211)	1.71 (indirect)
3-TBAF	a = 19.9390, b = 16.4070, c = 20.1470 α = 90.000, β = 97.563, γ = 90.000	2 x 2 x 2 (0.158 x 0.191 x 0.156)	2.49 (direct)

References:

1 A. Shaikh, S. Sahoo, S. R. Marder, S. Barlow and S. K. Mohapatra, *Org Biomol Chem*, 2024, **22**, 2115–2123.

2 S. K. Mohapatra, K. Al Kurdi, S. Jhulki, G. Bogdanov, J. Bacsa, M. Conte, T. V. Timofeeva, S. R. Marder and S. Barlow, *Beilstein J. Org. Chem.*, 2023, **19**, 1651–1663.

3 Z. H. Fu, J. C. Qin, Y. W. Wang, Y. Peng, Y. M. Zhang, D. M. Zhao and Z. H. Zhang, *Dyes and Pigments*, 2021, **185**, 108896.

4 P. R. Angarkhe, A. Shaikh, S. R. Rout, B. Sarma, J. Tripathy, R. Dandela and S. K. Mohapatra, *J Mol Str*, 2024, **1296**, 136920.

5 S. Chakraborty, R. Dutta, M. Arunachalam and P. Ghosh, *Dalton Transactions*, 2014, **43**, 2061–2068.

6 M. Arunachalam and P. Ghosh, *Chem Comm*, 2011, **47**, 6269–6271.

7 Q. Q. Wang, V. W. Day and K. Bowman-James, *Angew Chem Int Ed*, 2012, **51**, 2119–2123.

8 U. Manna, R. Chutia and G. Das, *Cryst Growth Des*, 2016, **16**, 2893–2903.

9 U. Manna, S. Kayal, B. Nayak and G. Das, *Dalton Transactions*, 2017, **46**, 11956–11969.

10 U. Manna and G. Das, *CrystEngComm*, 2018, **20**, 3741–3754.

11 S. Kumar, P. Shah, S. K. Tripathi, S. I. Khan and I. P. Singh, *Med Chem (Los Angeles)*, 2022, **18**, 949–969.

12 M. El Faydy, N. Dahaieh, K. Ounine, B. Lakhrissi, I. Warad, B. Tüzün and A. Zarrouk, *Arab J Sci Eng*, 2022, **47**, 497–510.

13 M. Adharvana Chari, D. Shobha and T. Sasaki, *Tetrahedron Lett*, 2011, **52**, 5575–5580.

14 G. M. Sheldrick, *Acta Cryst. A64*, 2008, 112–122.

15 G. Kresse and J. Furthmüller, *Phys Rev B*, 1996, **54**, 11169–11186.

16 G. Kresse and D. Joubert, *Phys Rev B*, 1999, **59**, 1758–1775.

17 Materials Design Inc., *MedeA Version 3.0; MedeA is a Registered Trademark of Materials Design, Inc.: San Diego, CA, USA. Available online: https://www.materialsdesign.com/medea-software*.

18 J. P. Perdew, K. Burke and M. Ernzerhof, *Phys Rev Lett*, 1996, **77**, 3865–3868.

19 H. J. Monkhorst and J. D. Pack, *Phys Rev B*, 1976, **13**, 5188–5192.